

ARTICLE OPEN



Improved strain engineering of 2D materials by adamantane plasma polymer encapsulation

Felix Carrascoso¹, Hao Li¹, Jose M. Obrero-Perez², Francisco J. Aparicio^{1,2,3}, Ana Borrás², Joshua O. Island⁴, Angel Barranco^{1,2}✉ and Andres Castellanos-Gomez¹✉

Two-dimensional materials present exceptional crystal elasticity and provide an ideal platform to tune electrical and optical properties through the application of strain. Here we extend recent research on strain engineering in monolayer molybdenum disulfide using an adamantane plasma polymer pinning layer to achieve unprecedented crystal strains of 2.8%. Using micro-reflectance spectroscopy, we report maximum strain gauge factors of -99.5 meV/% and -63.5 meV/% for the A and B exciton of monolayer MoS₂, respectively, with a 50 nm adamantane capping layer. These results are corroborated with photoluminescence and Raman measurements on the same samples. Taken together, our results indicate that adamantane polymer is an exceptional capping layer to transfer substrate-induced strain to a 2D layer and achieve higher levels of crystal strain.

npj 2D Materials and Applications (2023)7:24; <https://doi.org/10.1038/s41699-023-00393-1>

INTRODUCTION

Strain engineering is a powerful technique to modify the optical and electronic properties of two-dimensional (2D) materials through the deformation of their crystal lattice. 2D materials present an outstanding resilience to mechanical deformations allowing for a broad range of tunability through strain engineering^{1–8}. These strain properties have attracted great research interest but there are areas for further improvement and open challenges. In the vast majority of experiments relying on the deformation of a compliant flexible substrate, the strain transfer from substrate to crystal strongly depends on the Young's modulus of the substrate itself^{9,10}: the higher the substrate's Young's modulus the higher the realizable strain transfer. This is particularly critical as some flexible polymer substrates may present very low Young's modulus values, leading to an incomplete strain transfer from the deformed substrate to the 2D materials transferred on top. A second critical issue beyond this is that even when using substrates that ensure a good strain transfer, slippage of the flake typically limits the maximum strain that can be applied to roughly 0.8–1.4%¹¹. This slippage is determined by the tangential flake-substrate interactions and the total contact area^{12–14}. These problems have motivated the scientific community to find viable solutions.

One investigated solution is trying to mitigate slippage by clamping the 2D material to the flexible substrate with metal contacts¹⁵, so as to prevent the material from detaching from the substrate surface at high strain values. Nevertheless, this can lead to nonuniform strain that builds up at the contact locations and, unsurprisingly, relatively comparable uniaxial strain gauge factors have been obtained for MoS₂ in metal clamped and unclamped samples^{10,11,16–23}. Other works have tried to avoid slippage by covering the flake with a flexible polydimethylsiloxane (PDMS) layer^{24–26} or with a polymethylmethacrylate (PMMA) film²⁷; but a combination of large strain and gauge factor has not been obtained. An alternative and seemingly successful approach has

been to use a spin-coated polyvinyl alcohol (PVA) layer as a substrate²⁸. The spin-coated layer supposedly leads to better strain transfer through molecular bonding across the entire flake and at the edges. Using this technique, Li et al. found a large gauge factor of around -136 meV/% for single-layer MoS₂ but crystal strain was limited to 1.7%. Pressurized nano bubbles and blisters offer an alternative method to measure strain effects in 2D materials^{20,29,30}. While excessively large strains can be achieved, 5.6% in ref. ²⁰, this is non-uniform biaxial strain and the methods are less conducive to electrical transport measurements upon strain.

Here we implement a method to encapsulate 2D materials with nanometric films of adamantane (C₁₀H₁₆) plasma polymer to improve strain transfer and reduce slippage. Adamantane is the compound with the smallest cage structure of diamond crystal and was isolated from petroleum in 1933³¹. This material has been used in the field of medicine^{32,33}, and for various applications in coatings for smart electronic displays³⁴ and as molecular building blocks for nanostructure self-assembly³⁵. Adamantane plasma polymers were deposited at room temperature by solventless and scalable remote plasma-assisted vacuum deposition (RPAVD)^{36,37} using adamantane powder as precursor. These films present an extremely low roughness (RMS < 0.3 nm) and high transparency (bandgap 4.1 eV), thermal and chemical stability. Such properties together with the straightforward processing by dry etching and high conformality at the micro and nanoscale have prompted their applications in photonics^{38,39} and as protective layers for perovskite solar cells⁴⁰. It is also worth stressing that the fabrication in downstream configuration, i.e., out of the glow discharge, provides high compatibility with the deposition on molecular materials as supported organic nanowires and graphene⁴¹ without compromising their optical and electrical properties. In this work, we have deposited 50 nanometers of adamantane plasma polymer on top of several molybdenum disulfide (MoS₂) monolayers that were previously transferred onto flexible polycarbonate substrates to test the improvement of the

¹Materials Science Factory. Instituto de Ciencia de Materiales de Madrid (ICMM-CSIC), Madrid E-28049, Spain. ²Nanotechnology on Surfaces and Plasma Lab, Instituto de Ciencia de Materiales de Sevilla (CSIC-Universidad de Sevilla), C/Americo Vespucio 49, E-41092 Seville, Spain. ³Departamento de Física Aplicada I, Escuela Politécnica Superior, Universidad de Sevilla, c/ Virgen de África 7, E-41011 Seville, Spain. ⁴Department of Physics and Astronomy, University of Nevada Las Vegas, Las Vegas, NV 89154, USA.

✉email: angel.barranco@csic.es; andres.castellanos@csic.es

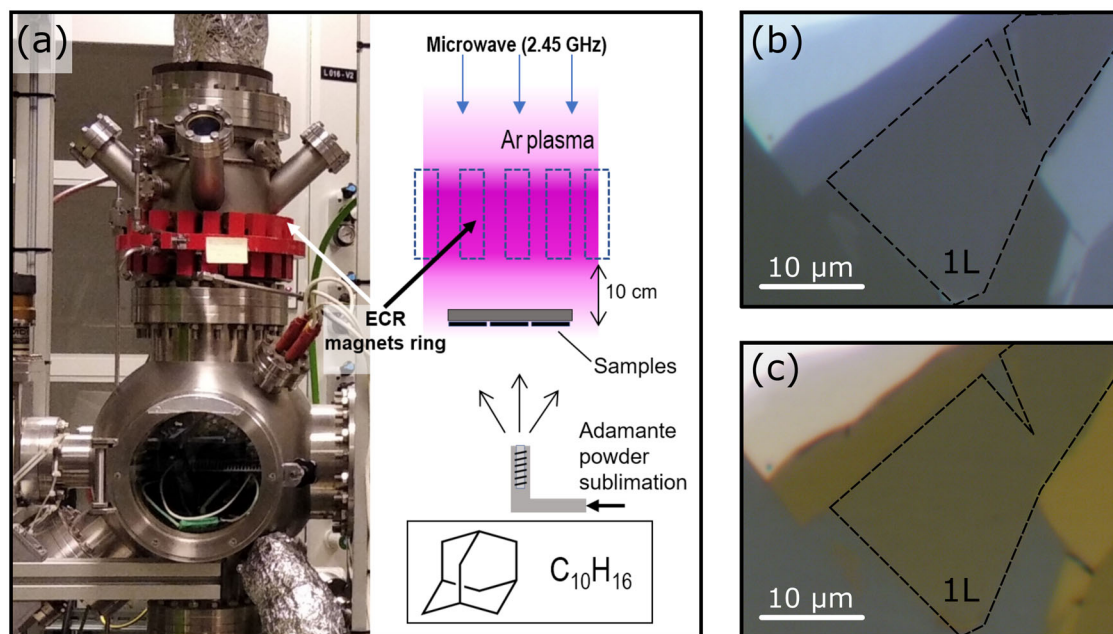


Fig. 1 Fabrication of adamantane encapsulated MoS₂ samples. **a** Experimental setup for the synthesis of adamantane plasma polymers by remote plasma-assisted vacuum deposition (RPAVD). The chemical structure and formula of adamantane are included in the top right part of panel **a**. **b** Optical image of 1L-MoS₂ on a polycarbonate substrate. **c** Same sample after encapsulating it with 50 nm of adamantane plasma polymer.

tunability of the bandgap of the material. We find a noticeable increase in the strain gauge factor for encapsulated flakes and reach unprecedented maximum crystal strains of 2.8%.

RESULTS

Sample fabrication

The adamantane polymer plasma encapsulation process consists of using remote plasma-assisted vacuum deposition (RPAVD) to deposit a thin layer of adamantane polymer through the controlled sublimation of adamantane powder in the downstream region of an Ar microwave electron cyclotron resonance (ECR) plasma (Fig. 1a). We address the reader to refs. ^{40,41} for full details about the plasma source and reactor geometry. We illustrate the utility of this encapsulation method by analyzing ten different single-layer MoS₂ samples. Figure 1b shows an optical image of a typical sample with a single-layer MoS₂ flake deposited onto a flexible polycarbonate (PC) substrate. We selected MoS₂ as it was one of the first isolated 2D semiconductors⁴² and the modification of its properties through crystal deformation has been widely investigated^{10,11,15,17–26,43–46}. This material consists of S-Mo-S layers that are held by weak van der Waal forces in a trigonal prismatic structure^{47–50}. In its bulk form, MoS₂ presents an indirect bandgap around 1.2 eV; however, a monolayer of this material exhibits a direct bandgap of 1.8 eV and displays a considerable in-plane charge carrier mobility and high current ON/OFF ratio when employed in a transistor⁵¹. These properties make molybdenum disulfide an attractive semiconductor for use in optical, electronic and straintronic applications.

Strain engineering experiments

We have directly compared the effect of the adamantane encapsulation on the strain tunability of the optical properties of a single-layer MoS₂ flake. Figure 2 shows the micro-reflectance spectra of a single-layer MoS₂ flake by employing the three-point bending setup to bend the PC substrate to strain the 2D crystal (additional data sets for other flakes can be found in Supplementary Figs. 1–8). Figure 2a presents the spectra acquired at different

strain values before and after encapsulating the sample. The spectra exhibit two prominent peaks that correspond to the A and B excitons at around 1.9 eV and 2.0 eV and correspond to the direct bandgap transition at the K point of the Brillouin zone in monolayer MoS₂^{52–56}. It should be noted that the differential reflectance spectra obtained after encapsulating the sample are inverted due to the interference phenomena explained by a Fresnel-law-based model when one has a multilayer optical media with different refractive indexes⁵⁷. Figure 2b shows the energy of the A and B peak positions as a function of the applied uniaxial strain before and after encapsulation. The slope of the linear trend followed by the experimental datapoints indicates the strain gauge factor (the change in exciton energy per % of uniaxial strain) for both excitons, being -42.7 ± 1.9 meV/% and -47.4 ± 5.5 meV/% for the A and B exciton, respectively, without encapsulation and -76.6 ± 1.5 meV/% and -59.1 ± 4.6 meV/% after depositing 50 nm of adamantane plasma polymer onto the sample. These values indicate that the gauge factor after the encapsulation process has increased by 24% and a 34% for the A and the B exciton, respectively.

Figure 3 shows the statistical information obtained after measuring ten different single-layer MoS₂ flakes (see the Supporting Information for data sets for other flakes, Supplementary Figs. 1–8) for the gauge factors of the A and B excitons. Black dots show those samples that were measured before the encapsulation process, blue dots indicate the measured samples after encapsulating them with 50 nm of adamantane polymer film and the gray dots correspond to data collected from other 15 un-encapsulated single-layer MoS₂ samples reported in our previous work¹¹. We can observe an overall improved strain tunability for the encapsulated samples, which is attributed to the fact that the strain is being transferred more effectively to the single-layer MoS₂ flakes. Note that the orange dots in Fig. 3 refer to the same sample that was tested in Fig. 2 after being subjected to several straining tests and forcing it to the failure limit (these results will be displayed in Fig. 4). These data demonstrate an increment in the gauge factor between a 24% and a 214% for the A exciton and between a 24% and a 253% for the B exciton, obtaining a

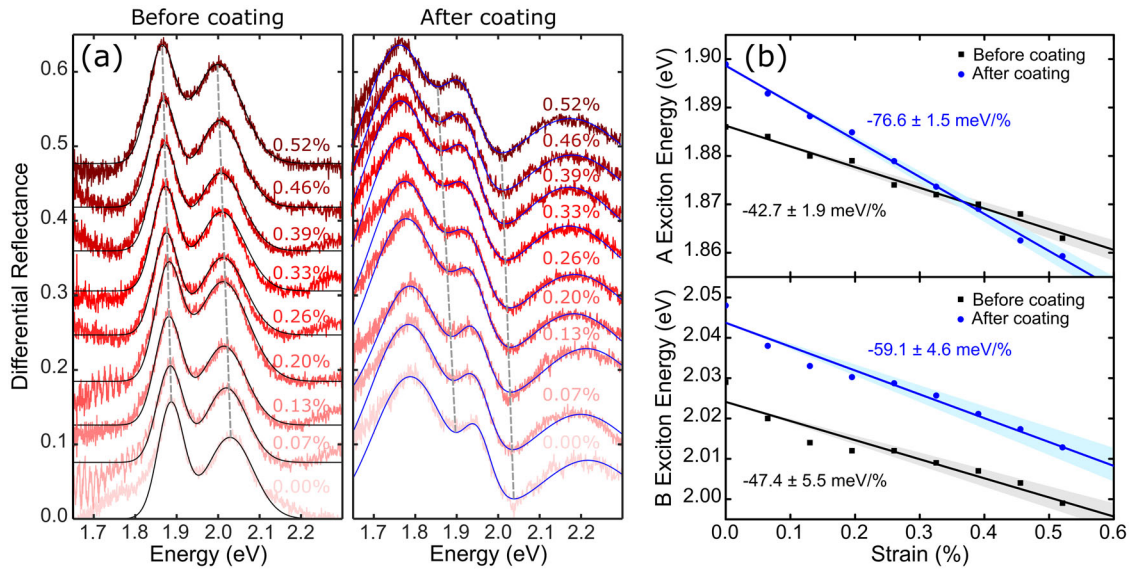


Fig. 2 Strain tunable reflectance. **a** Differential reflectance spectra at different uniaxial strain values of a single-layer MoS₂ flake before and after adamantane plasma polymer encapsulation. **b** A and B exciton energies at different uniaxial strain values before and after adamantane plasma polymer encapsulation. The data has been fit to a straight line to extract the gauge factor value (solid line). The shaded area around the solid line indicates the uncertainty of the fit.

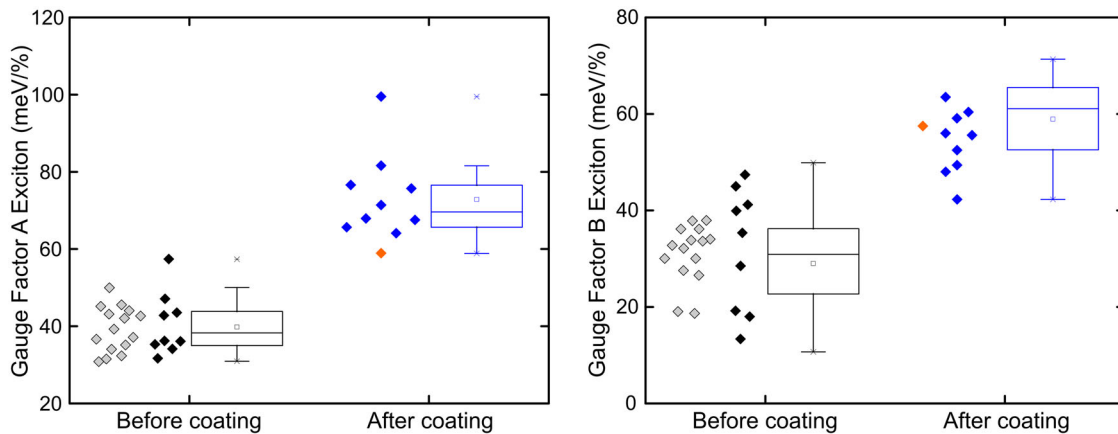


Fig. 3 Statistical flake-to-flake variation of the gauge factor. Statistical flake-to-flake variation before encapsulation (black and grey dots) and after encapsulation (blue dots). Grey dots correspond to other 15 un-encapsulated samples that were measured in our previous work¹¹. Orange dots refer to the same sample that was tested in Fig. 2 after being subjected to several reproducibility cycles and testing it till the device failure.

maximum gauge factor of -99.5 meV/% for the A exciton and -63.5 meV/% for the B exciton. One could attribute this improved gauge factor to the large Young's modulus of 7.5 ± 0.3 GPa of the adamantane plasma polymer films (see the Supplementary Fig. 9). However, we have fabricated a 1L-MoS₂ sample on a polycarbonate substrate coated with a 50 nm thick adamantane plasma polymer finding a gauge factor compatible with that of bare polycarbonate. Interestingly, after encapsulating that sample with another 50 nm thick adamantane film one recover again the improved gauge factor (Supplementary Fig. 10). This indicates us that the improved strain transfer is not simply due to the high Young's modulus of the adamantane plasma polymer film but that the encapsulation process is crucial to explain it. We have experimentally verified that the adamantane-substrate adhesion is so strong that once this film is formed, it cannot be separated from the substrate by physical methods (sonication, heating, scotch tape test, etc.). This strong adhesion with a material with high Young's modulus could explain the improved strain transfer

and also reduced slippage. Other plausible source for reduced slippage could be chemical interaction between the adamantane and defects. As the deposition conditions have been carefully chosen to avoid ion bombardment and ultraviolet light exposure to the MoS₂ flakes, we believe that chemical interaction of the adamantane plasma polymer with the MoS₂, which could act as clamping points, should be only possible at the intrinsic defect sites within the MoS₂ layer or at the edges. Note that although Li et al. found larger gauge factors (around -136 meV/%) for two MoS₂ samples using a PVA encapsulation and peeling-off method²⁸; we attempted to improve the gauge factor of our samples by encapsulating MoS₂, deposited onto PC, with PVA on top without success (see the Supplementary Fig. 10). This motivated our use of adamantane polymer films to improve the strain transfer in monolayer MoS₂ samples.

In Fig. 4, we subject a single-layer MoS₂ flake to very high strain values to determine the maximum strain before slippage. Panel a and b shows the A peak position and the B peak position as a

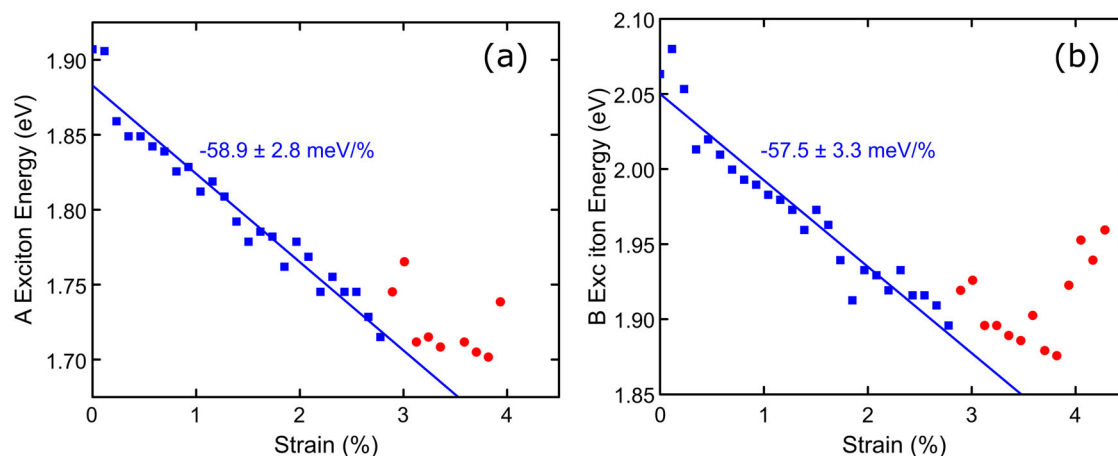


Fig. 4 Maximum achievable strain. **a, b** A and B exciton energies, respectively, of a single-layer MoS₂ flake at different uniaxial strain values after adamantane plasma polymer encapsulation. The straining test has been carried out until the failure of the device. The blue squares and red dots correspond to the datapoints acquired before and after the flake starts to slip, respectively.

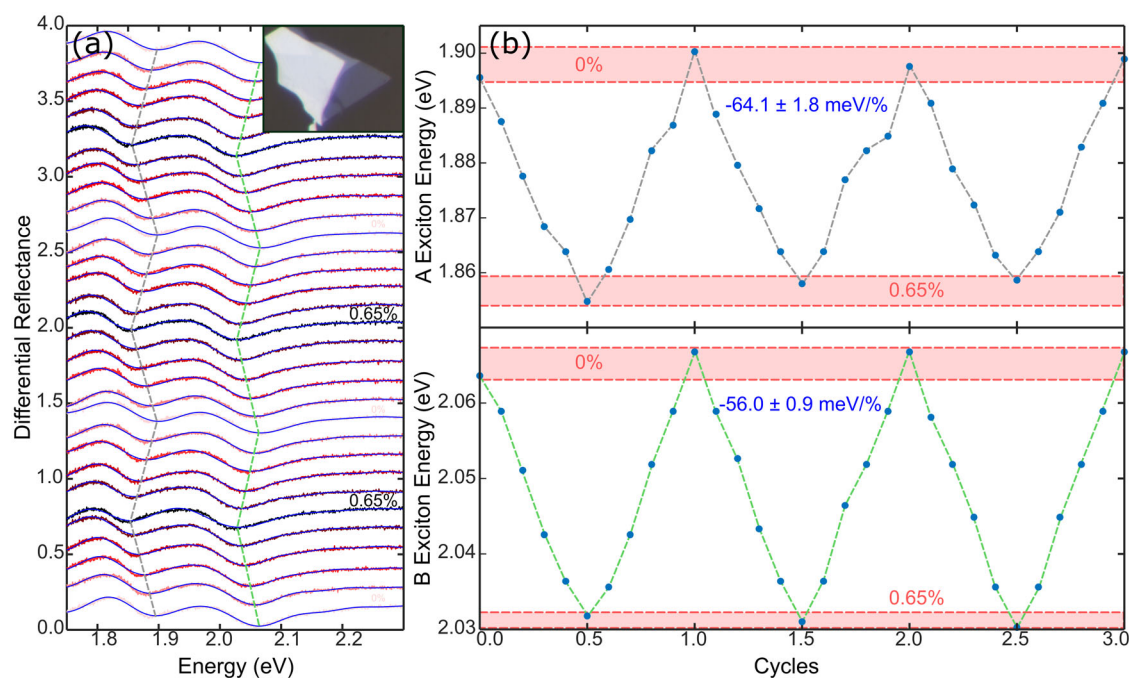


Fig. 5 Reproducibility of straining experiments. **a** Differential reflectance spectra acquired at different uniaxial strain values, up to 0.65%, to probe its reproducibility. **b** A and B exciton energies for the different strain cycles between 0 and 0.65%.

function of the applied uniaxial strain, respectively. We can observe a clear linear behavior from 0 to 2.8% (blue dots), at which point the flake starts to slip and release strain as can be seen from the occurrence of sudden upward jumps in the exciton energy and the reduced slope (red dots). Another four adamantane plasma polymer coated samples, see the Supporting Information (Supplementary Figs. 11–14), reached a maximum strain ranging between 1.7 and 2.4%. These maximum strain values with the adamantane polymer encapsulation are very promising given that un-encapsulated samples show signs of slippage for strains between 0.8 and 1.4%¹¹. Our adamantane layer is ideal even when compared with the PVA encapsulation and peeling-off method given that the maximum reported strain value for a single MoS₂ sample was 1.7%²⁸.

We also tested the reproducibility of these measurements (see Fig. 5). We applied three straining/releasing cycles on a single-

layer MoS₂ flake after being encapsulated with 50 nm of adamantane (optical picture in the inset). Panel a presents the spectra acquired during this cycling process and panel b summarizes the energy of the A and B peaks as a function of the applied uniaxial strain from 0% to 0.65%, showing a good agreement between the subsequent cycles. Another example of reproducibility test is shown in the Supplementary Fig. 16 where 14 straining (~1%)/releasing (0%) cycles are summarized.

To corroborate our micro-reflectance spectra data, we also acquired photoluminescence and Raman spectra of a single layer MoS₂ flake as a function of the applied strain. Figure 6a) shows photoluminescence spectra before and after depositing 50 nm of adamantane, and the A peak position vs. the strain value can be observed in Fig. 6b. Gauge factors of -37.1 ± 3.0 meV/% and -70.2 ± 7.3 meV/% were obtained before and after the encapsulation, respectively. See Supplementary Fig. 17 for another

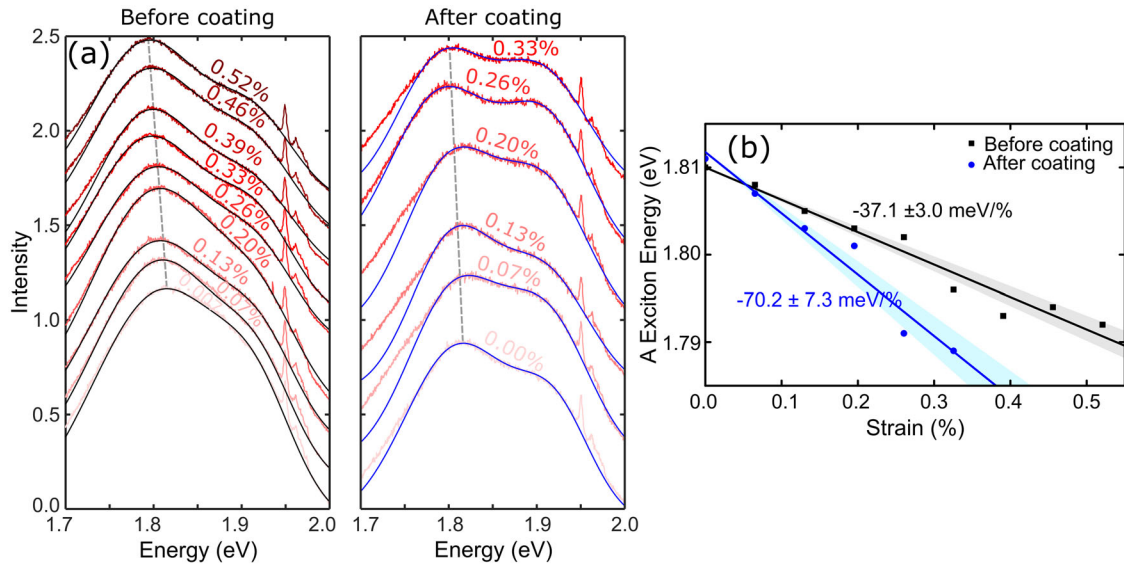


Fig. 6 Strain tunable photoluminescence. **a** Photoluminescence spectra acquired for different uniaxial strains on a single-layer MoS₂ flake before and after adamantane plasma polymer encapsulation. **b** A exciton energy as a function of uniaxial strain before and after encapsulation. The data has been fit to a straight line to extract the gauge factor value (solid line). The shaded area around the solid line indicates the uncertainty of the fit.

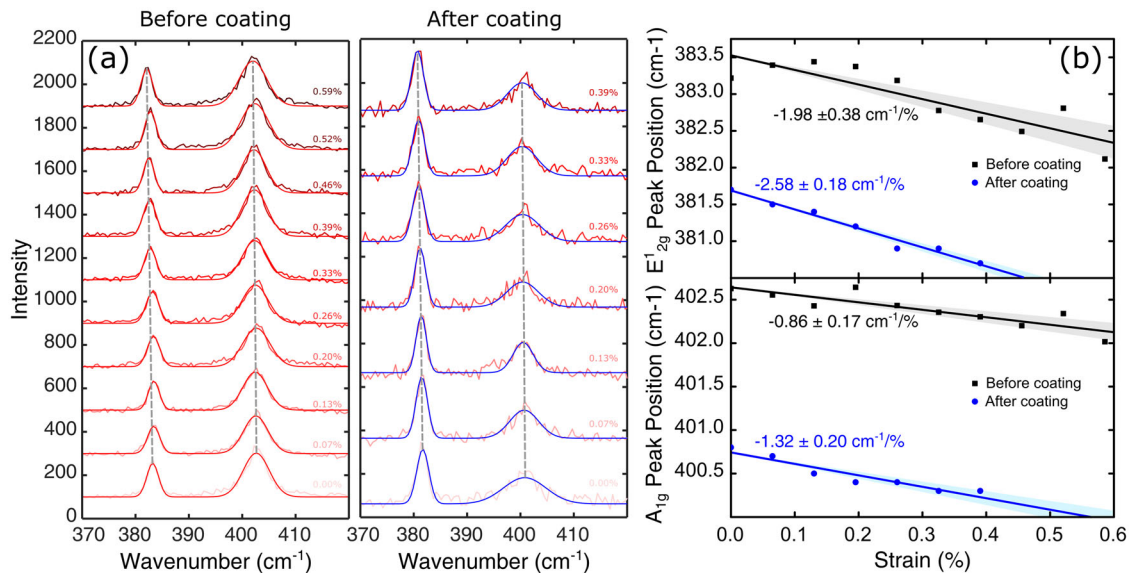


Fig. 7 Strain tunable Raman. **a** Raman spectra acquired for different uniaxial strains on a single-layer MoS₂ flake before and after adamantane plasma polymer encapsulation. **b** E'_{2g} and A_{1g} peak positions as a function of uniaxial strain before and after encapsulation. The data has been fit to a straight line to extract the gauge factor value (solid line). The shaded area around the solid line indicates the uncertainty of the fit.

photoluminescence dataset in an adamantane encapsulated 1L-MoS₂. A remarkable increase in the gauge factor is appreciated, which agrees with the obtained micro-reflectance measurements. Notably, we observe a global offset in the A exciton energy position in the photoluminescence measurements in comparison to the micro-reflectance spectroscopy experiments. We associate this shift to the broad background signal in the photoluminescence measurements that is produced by the substrate and to the Stokes shift⁵⁸. Supplementary Fig. 18 in the Supporting Information also compares the strain evolution of the photoluminescence A exciton peak full-width-at-half-maximum upon straining.

In Fig. 7 we present Raman spectra of a monolayer MoS₂ flake following the same methodology. Figure 7a shows the Raman

spectra that were obtained before and after 50 nm adamantane film encapsulation as a function of different uniaxial strain values where E'_{2g} and A_{1g} peaks for MoS₂ can be clearly observed. Figure 7b displays the peak position vs. the applied strain before and after encapsulation and a noticeable increase of the gauge factor for both peaks is detected. We note that a global shift in the Raman peaks at 0 % strain is recorded in these measurements. This points to possible built-in crystal strain (compression) after the deposition of adamantane. This is supported by our micro-reflectance measurements as well, which also display a shift in the exciton peak positions after adamantane deposition. We also note a broadening of the A_{1g} peak, which may indicate some varying of the monolayer force constants, as expected for an atomically thin

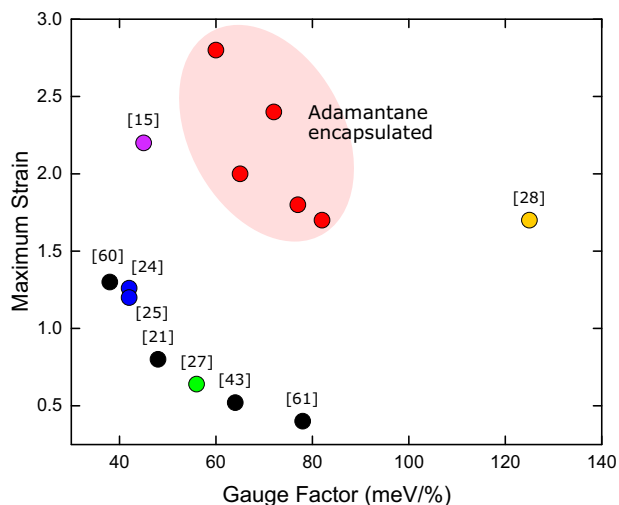


Fig. 8 Comparison between the strain engineering experiments in the literature. Maximum strain versus gauge factor in single-layer MoS₂. Red dots: results obtained in this work. Black dots: bare monolayers from other works^{21,43,60,61}. Blue dots: monolayers covered with a PDMS film^{24,25}. Purple dot: monolayer MoS₂ flake clamped to the substrate with a metal contact¹⁵. Green dot: single-layer MoS₂ encapsulated with a PMMA film²⁷. Yellow dot: monolayer MoS₂ covered with a PVA coating²⁸.

material when it is covered with another material with which feels an interatomic interaction (e.g. adhesion). In fact, a similar broadening is observed when comparing monolayer and bilayer MoS₂ samples because of the interaction of the topmost MoS₂ layer with the bottom layer⁵⁹. Although the broadening of Raman peaks can be sometimes attributed to the presence of defects, we note that the adamantane deposition process conditions were precisely determined to avoid ion bombardment and ultraviolet light interaction with the substrate surface during deposition. Moreover, after deposition we do not observe a sizeable decrease on the quality of the PL or the differential reflectance spectra indicating that, if defects are induced, their density and effect on the optical properties of the encapsulated MoS₂ are low. Supplementary Fig. 19 in the Supporting Information summarizes the full-width-at-half-maximum of the Raman peaks, before and after adamantane coating, upon strain.

Comparison between different strain engineering experiments in literature

Figure 8 summarizes the maximum reported gauge factor and maximum achieved strain before slippage in uniaxial strain engineering experiments with single-layer MoS₂. By comparing with other experiments one can see how adamantane coating yields a good combination of large gauge factor and large maximum strain value. Black data points indicate data points acquired on bare (un-encapsulated or un-clamped) MoS₂ monolayers^{21,43,60,61}; blue data points correspond to those samples that were covered with a PDMS film to avoid the slippage^{24,26}; purple data point corresponds to the clamped sample¹⁵; the green data point indicates a single-layer MoS₂ flake that was encapsulated with a PMMA film²⁷; and the yellow data point corresponds to the sample covered with a PVA coating²⁸. As we can observe, the adamantane plasma polymer-coated samples have a good balance of high gauge factor and large maximum strain leading to a large band gap tunability. We further note that the adamantane-coated MoS₂ data were obtained after the samples were subjected to multiple straining tests, so the gauge factors and the maximum strain values could be lower than those that would have been obtained in a pristine sample.

DISCUSSION

In summary, we present a method to encapsulate two-dimensional materials with adamantane polymer layer that contributes to transfer the strain from the substrate to the flake more efficiently. The deposition process allows for the simultaneous conformal deposition of multiple devices in a solventless, room-temperature process. We demonstrate the performance of this technique by studying ten single-layer MoS₂ samples subjected to uniaxial strain before and after the adamantane polymer encapsulation. We find a higher gauge factor in all the studied samples after encapsulation. We have used differential reflectance spectroscopy, finding gauge factors ranging from -58.9 meV/% to -99.5 meV/% for the A peak and -49.4 meV/% to -63.5 meV/% for the B peak after encapsulation, which is considerably higher than those gauge factors that were obtained without any encapsulation, ranging from -31.0 meV/% to -57.4 meV/% for the A exciton and -18.0 meV/% to -47.4 meV/% for the B exciton. We have also found that, after depositing the adamantane film, a value of 2.8% of uniaxial strain can be achieved before slippage occurs. This value is approximately twice the maximum uniaxial strain values commonly found in un-encapsulated samples. We also tested the reproducibility of the measurements by subjecting a sample to various strain cycles, finding a good reproducibility between cycles. In addition, we have obtained photoluminescence and Raman spectra under strain to corroborate the measurements that were obtained with micro-reflectance spectroscopy. Finally, taken all together, our results show that adamantane plasma polymer encapsulation is an attractive method of encapsulation that gives rise to higher strain transfer and increases the maximum crystal strain that can be achieved in experiments. Our method advances development in strain engineering of materials and can be readily applied to other members of the interesting class of 2D materials.

METHODS

Straining setup and experiments

We employ a three-point bending setup for applying uniaxial strain because we have found that a two-point bending rig leads to sample repositioning and refocusing with application of strain^{11,17}. In addition, and as identified in our previous work, slippage is more common in uniaxial strain than in biaxial strain experiments¹⁷. It is therefore advantageous to develop an effective encapsulation process that mitigates slippage in uniaxial strain experiments. Accordingly, we carry out the same experiment before and after the adamantane deposition in order to test the efficiency of the encapsulation. All information about the calibration of this setup can be found in our previous work¹¹.

Sample fabrication

The fabrication of the MoS₂ samples consists of exfoliating bulk MoS₂ crystals (Molly Hill mine, Quebec, Canada) with Nitto tape (SPV224) and transferring the obtained flakes onto a Gel-Film substrate (WfX4 6.0 mil, by Gel-Pak®). By using the micro-reflectance spectroscopy method^{54,62}, which allows us to determine the thickness of the crystals, we select a single-layer MoS₂ flake and we place it onto the center of a beam-shaped, 250 μ m thick polycarbonate (PC) substrate using an all dry deterministic transfer method^{63–65}.

Adamantane encapsulation process

The encapsulation process consists of using remote plasma-assisted vacuum deposition (RPAVD) to deposit a thin layer of adamantane plasma polymer to the surface of the sample. RPAVD is a useful method to deposit polymer-like layers of sensitive functional organic molecules that cannot be deposited in a direct

Ar plasma due to excessive precursor fragmentation. Adamantane powder (>99%) was purchased from Sigma-Aldrich and used as received. The deposition process consists of the controlled sublimation of adamantane powder in the downstream region of an Ar microwave electron cyclotron resonance (ECR) plasma. The deposition pressure was 10^{-2} mbar and the plasma power was 150 W. The temperature of the substrates was 10–15 °C above room temperature, determined by a thermocouple connected to the sample holder in the same position as the substrates. In an ECR plasma, the discharge is mostly confined in the region inside the magnet ring (in red in the picture shown in Fig. 1a). The sample holder was placed about ~10 cm from the base of the magnet ring, as indicated in the schematic in the figure, and oriented upside down to reduce plasma interaction with the surface. The evaporation rate was monitored with a calibrated quartz crystal monitor (QCM). A set of films examined by spectroscopic ellipsometry was used to calibrate the QCM values to obtain reproducible thickness values. Besides, reference films on Si(100) were examined by spectroscopy ellipsometry to check the thickness in each deposition process. Full details regarding the plasma source and reactor geometry can be found elsewhere^{40,41}. Figure 1b shows an optical image of the single-layer MoS₂ flake before encapsulation and Fig. 1c shows the flake after deposition of 50 nm of adamantane. A contrast and color difference can be readily appreciated across the entire sample.

Ellipsometry

Variable angle spectroscopy ellipsometry was carried out with a VASE ellipsometer from J.A. Woollan Co.

Mechanical measurements

Young modulus values were obtained in a NanoXP nanoindenter from MTS Nanosystems using the continuous stiffness (CSM) and low load dynamic contact (DCM) modules. The study was carried out using $5 \times 1 \text{ cm}^2$ ~500 nm thick adamantane plasma samples prepared in identical conditions on Si(100) and fused silica. The values obtained corresponded to a total of 70 indentations.

DATA AVAILABILITY

The datasets generated during and/or analysed during the current study are available from the authors on reasonable request.

Received: 8 August 2022; Accepted: 10 March 2023;

Published online: 30 March 2023

REFERENCES

- Roldán, R., Castellanos-Gomez, A., Cappelluti, E. & Guinea, F. Strain engineering in semiconducting two-dimensional crystals. *J. Phys.: Condens. Matter.* **27**, 313201 (2015).
- Amorim, B. et al. Novel effects of strains in graphene and other two dimensional materials. *Phys. Rep.* **617**, 1–54 (2016).
- Deng, S., Sumant, A. V. & Berry, V. Strain engineering in two-dimensional nanomaterials beyond graphene. *Nano Today* **22**, 14–35 (2018).
- Dai, Z., Liu, L. & Zhang, Z. Strain engineering of 2D materials: issues and opportunities at the interface. *Adv. Mater.* **31**, 1805417 (2019).
- Sun, Y. & Liu, K. Strain engineering in functional 2-dimensional materials. *J. Appl. Phys.* **125**, 082402 (2019).
- Huang, T., Wei, W., Chen, X. & Dai, N. Strained 2D layered materials and heterojunctions. *Ann. Phys.* **531**, 1800465 (2019).
- Peng, Z., Chen, X., Fan, Y., Srolovitz, D. J. & Lei, D. Strain engineering of 2D semiconductors and graphene: from strain fields to band-structure tuning and photonic applications. *Light Sci. Appl.* **9**, 190 (2020).
- Chaves, A. et al. Bandgap engineering of two-dimensional semiconductor materials. *Npj 2D Mater. Appl.* **4**, 29 (2020).
- Liu, Z. et al. Strain and structure heterogeneity in MoS₂ atomic layers grown by chemical vapour deposition. *Nat. Commun.* **5**, 5246 (2014).
- Frisenda, R. et al. Biaxial strain tuning of the optical properties of single-layer transition metal dichalcogenides. *Npj 2D Mater. Appl.* **1**, 10 (2017).
- Carrascoso, F., Li, H., Frisenda, R. & Castellanos-Gomez, A. Strain engineering in single-, bi- and tri-layer MoS₂, MoSe₂, WS₂ and WSe₂. *Nano Res.* **14**, 1698–1703 (2021).
- Dai, Z. et al. Mechanical behavior and properties of hydrogen bonded graphene/polymer nano-interfaces. *Compos. Sci. Technol.* **136**, 1–9 (2016).
- Papageorgiou, D. G., Kinloch, I. A. & Young, R. J. Mechanical properties of graphene and graphene-based nanocomposites. *Prog. Mater. Sci.* **90**, 75–127 (2017).
- Dai, Z., Lu, N., Liechti, K. M. & Huang, R. Mechanics at the interfaces of 2D materials: challenges and opportunities. *Curr. Opin. Solid State Mater. Sci.* **24**, 100837 (2020).
- Conley, H. J. et al. Bandgap engineering of strained monolayer and bilayer MoS₂. *Nano Lett.* **13**, 3626–3630 (2013).
- Gant, P. et al. A system for the deterministic transfer of 2D materials under inert environmental conditions. *2D Mater.* **7**, 025034 (2020).
- Carrascoso, F., Frisenda, R. & Castellanos-Gomez, A. Biaxial versus uniaxial strain tuning of single-layer MoS₂. *Nano Mater. Sci.* **4**, 44–51 (2022).
- Ryu, Y. K. et al. Microheater actuators as a versatile platform for strain engineering in 2D materials. *Nano Lett.* **20**, 5339–5345 (2020).
- Hui, Y. Y. et al. Exceptional tunability of band energy in a compressively strained trilayer MoS₂ sheet. *ACS Nano* **7**, 7126–7131 (2013).
- Lloyd, D. et al. Band gap engineering with ultralarge biaxial strains in suspended monolayer MoS₂. *Nano Lett.* **16**, 5836–5841 (2016).
- Zhu, C. R. et al. Strain tuning of optical emission energy and polarization in monolayer and bilayer MoS₂. *Phys. Rev. B* **88**, 121301 (2013).
- Plechinger, G. et al. Control of biaxial strain in single-layer molybdenite using local thermal expansion of the substrate. *2D Mater.* **2**, 015006 (2015).
- Gant, P. et al. A strain tunable single-layer MoS₂ photodetector. *Mater. Today* **27**, 8–13 (2019).
- Niehues, I. et al. Strain control of exciton-phonon coupling in atomically thin semiconductors. *Nano Lett.* **18**, 1751–1757 (2018).
- Niehues, I., Blob, A., Stiehm, T. & de Vasconcellos, S. M. Interlayer excitons in bilayer MoS₂ under uniaxial tensile strain. *Nanoscale* **11**, 12788–12792 (2019).
- Niehues, I. et al. Strain transfer across grain boundaries in MoS₂ monolayers grown by chemical vapor deposition. *2D Mater.* **5**, 31003 (2018).
- He, X. et al. Strain engineering in monolayer WS₂, MoS₂, and the WS₂/MoS₂ heterostructure. *Appl. Phys. Lett.* **109**, 173105 (2016).
- Li, Z. et al. Efficient strain modulation of 2D materials via polymer encapsulation. *Nat. Commun.* **11**, 1–8 (2020).
- Tedeschi, D. et al. Controlled micro/nanodome formation in proton-irradiated bulk transition-metal dichalcogenides. *Adv. Mater.* **31**, 1903795 (2019).
- Blundo, E. et al. Evidence of the direct-to-indirect band gap transition in strained two-dimensional WS₂, MoS₂, and WSe₂. *Phys. Rev. Res.* **2**, 012024 (2020).
- Fort, R. C. & Von Schleyer, P. R. Adamantane: Consequences of the Diamondoid Structure. *Chem. Rev.* **64**, 277–300 (1964).
- Lamoureux, G. & Artavia, G. Use of the adamantane structure in medicinal chemistry. *Curr. Med. Chem.* **17**, 2967–2978 (2010).
- Wishnok, J. S. Medicinal properties of adamantane derivatives. *J. Chem. Educ.* **50**, 780–789 (1973).
- Jeong, H. Y. et al. Synthesis and characterization of the first adamantane-based poly(p-phenylenevinylene) derivative: an intelligent plastic for smart electronic displays. *Thin Solid Films* **417**, 171–174 (2002).
- García, J. C., Justo, J. F., MacHado, W. V. M. & Assali, L. V. C. Functionalized adamantane: building blocks for nanostructure self-assembly. *Phys. Rev. B - Condens. Matter Mater. Phys.* **80**, 125421 (2009).
- Błaszczak-Lezak, I. et al. Optically active luminescent perylene thin films deposited by plasma polymerization. *J. Phys. Chem. C* **113**, 431–438 (2009).
- Barranco, A. & Groening, P. Fluorescent plasma nanocomposite thin films containing nonaggregated rhodamine 6G laser dye molecules. *Langmuir* **22**, 6719–6722 (2006).
- Aparicio, F. J. et al. Plasma deposition of perylene–adamantane nanocomposite thin films for NO₂ room-temperature optical sensing. *J. Phys. Chem. C* **116**, 8731–8740 (2012).
- Alcaire, M. et al. Multicolored emission and lasing in DCM-adamantane plasma nanocomposite optical films. *ACS Appl. Mater. Interfaces* **9**, 8948–8959 (2017).
- Idigoras, J. et al. Enhancing moisture and water resistance in perovskite solar cells by encapsulation with ultrathin plasma polymers. *ACS Appl. Mater. Interfaces* **10**, 11587–11594 (2018).
- Alcaire, M. et al. Plasma enabled conformal and damage free encapsulation of fragile molecular matter: from surface-supported to on-device nanostructures. *Adv. Funct. Mater.* **29**, 1903535 (2019).
- Novoselov, K. S. et al. Two-dimensional atomic crystals. *Proc. Natl Acad. Sci. USA* **102**, 10451–10453 (2005).

43. He, K., Poole, C., Mak, K. F. & Shan, J. Experimental demonstration of continuous electronic structure tuning via strain in atomically thin MoS₂. *Nano Lett.* **13**, 2931–2936 (2013).
44. Carrascoso, F., Lin, D.-Y., Frisenda, R. & Castellanos-Gomez, A. Biaxial strain tuning of interlayer excitons in bilayer MoS₂. *J. Phys. Mater.* **3**, 015003 (2019).
45. Island, J. O. et al. Precise and reversible band gap tuning in single-layer MoSe₂ by uniaxial strain. *Nanoscale* **8**, 2589–2593 (2016).
46. Scalise, E., Houssa, M., Pourtois, G., Afanas'ev, V. & Stesmans, A. Strain-induced semiconductor to metal transition in the two-dimensional honeycomb structure of MoS₂. *Nano Res.* **5**, 43–48 (2011).
47. Verble, J. L. & Wieting, T. J. Lattice mode degeneracy in MoS₂ and other layer compounds. *Phys. Rev. Lett.* **25**, 362–365 (1970).
48. Mattheiss, L. F. Band structures of transition-metal-dichalcogenide layer compounds. *Phys. Rev. B* **8**, 3719–3740 (1973).
49. Coehoorn, R. et al. Electronic structure of MoSe₂, MoS₂, and WSe₂. I. Band-structure calculations and photoelectron spectroscopy. *Phys. Rev. B* **35**, 6195–6202 (1987).
50. Joensen, P., Frindt, R. F. & Morrison, S. R. Single-layer MoS₂. *Mater. Res. Bull.* **21**, 457–461 (1986).
51. Radisavljevic, B., Radenovic, A., Brivio, J., Giacometti, V. & Kis, A. Single-layer MoS₂ transistors. *Nat. Nanotechnol.* **6**, 147–150 (2011).
52. Mak, K. F., Lee, C., Hone, J., Shan, J. & Heinz, T. F. Atomically thin MoS₂: a new direct-gap semiconductor. *Phys. Rev. Lett.* **105**, 136805 (2010).
53. Splendiani, A. et al. Emerging photoluminescence in monolayer MoS₂. *Nano Lett.* **10**, 1271–1275 (2010).
54. Niu, Y. et al. Thickness-dependent differential reflectance spectra of monolayer and few-layer MoS₂, MoSe₂, WS₂ and WSe₂. *Nanomaterials* **8**, 725 (2018).
55. Chernikov, A. et al. Exciton binding energy and nonhydrogenic rydberg series in monolayer WS₂. *Phys. Rev. Lett.* **113**, 076802 (2014).
56. Castellanos-Gomez, A., Querada, J., van der Meulen, H. P., Agraït, N. & Rubio-Bollinger, G. Spatially resolved optical absorption spectroscopy of single- and few-layer MoS₂ by hyperspectral imaging. *Nanotechnology* **27**, 115705 (2016).
57. Blake, P. et al. Making graphene visible. *Appl. Phys. Lett.* **91**, 063124 (2007).
58. Liu, B. et al. Engineering bandgaps of monolayer MoS₂ and WS₂ on fluoropolymer substrates by electrostatically tuned many-body effects. *Wiley Online Libr.* **28**, 6457–6464 (2016).
59. Lee, C. et al. Anomalous lattice vibrations of single- and few-layer MoS₂. *ACS Nano* **4**, 2695–2700 (2010).
60. Christopher, J. W. et al. Monolayer MoS₂ strained to 1.3% with a microelectromechanical system. *J. Microelectromech. Syst.* **28**, 254–263 (2019).
61. John, A. P., Thenapparambil, A. & Thalakulam, M. Strain-engineering the Schottky barrier and electrical transport on MoS₂. *Nanotechnology* **31**, 275703 (2020).
62. Frisenda, R. et al. Micro-reflectance and transmittance spectroscopy: a versatile and powerful tool to characterize 2D materials. *J. Phys. Appl. Phys.* **50**, 074002 (2017).
63. Frisenda, R. et al. Recent progress in the assembly of nanodevices and van der Waals heterostructures by deterministic placement of 2D materials. *Chem. Soc. Rev.* **47**, 53–68 (2018).
64. Castellanos-Gomez, A. et al. Deterministic transfer of two-dimensional materials by all-dry viscoelastic stamping. *2D Mater.* **1**, 011002 (2014).
65. Yang, R., Zheng, X., Wang, Z., Miller, C. J. & Feng, P. X.-L. Multilayer MoS₂ transistors enabled by a facile dry-transfer technique and thermal annealing. *J. Vac. Sci. Technol. B Nanotechnol. Microelectron. Mater. Process. Meas. Phenom.* **32**, 61203 (2014).

ACKNOWLEDGEMENTS

A.C.G. acknowledges funding from the European Research Council (ERC) under the European Union's Horizon 2020 research and innovation program (Grant Agreement No. 755655, ERC-StG 2017 project 2D-TOPSENSE), the EU FLAG-ERA project To2Dox (JTC-2019-009) and the Comunidad de Madrid through the CAIRO-CM project (Y2020/NMT-6661). Ana B. thanks the ERC Union's Horizon 2020 program (Grant Agreement No. 851929 StG 2019 project 3DScavengers). We also thank the Spanish Ministry of Science and Innovation AEI/10.13039/501100011033 (grants PID2020-115566RB-I00, TED2021-132267B-I00 and PID2019-110430GB-C21), the EU ERDF (FEDER Operational Program (2014-2020), A way of making Europe) and the Consejería de Economía, Conocimiento, Empresas y Universidad de la Junta de Andalucía (de grants P18-RT-3480, EMERGIA and US-1381057).

AUTHOR CONTRIBUTIONS

F.C. and H.L. fabricated 1L MoS₂ samples and performed uniaxial strain tests. J.M.O.-P., F.J.A., Ana B., and Angel B., performed the deposition of the adamantane and the characterization of its Young's modulus. J.O.I. and A.C.-G. wrote the first draft of the manuscript, all co-authors contributed to the final version of the manuscript.

COMPETING INTERESTS

The authors declare no competing interests.

ADDITIONAL INFORMATION

Supplementary information The online version contains supplementary material available at <https://doi.org/10.1038/s41699-023-00393-1>.

Correspondence and requests for materials should be addressed to Angel Barranco or Andres Castellanos-Gomez.

Reprints and permission information is available at <http://www.nature.com/reprints>

Publisher's note Springer Nature remains neutral with regard to jurisdictional claims in published maps and institutional affiliations.



Open Access This article is licensed under a Creative Commons Attribution 4.0 International License, which permits use, sharing, adaptation, distribution and reproduction in any medium or format, as long as you give appropriate credit to the original author(s) and the source, provide a link to the Creative Commons license, and indicate if changes were made. The images or other third party material in this article are included in the article's Creative Commons license, unless indicated otherwise in a credit line to the material. If material is not included in the article's Creative Commons license and your intended use is not permitted by statutory regulation or exceeds the permitted use, you will need to obtain permission directly from the copyright holder. To view a copy of this license, visit <http://creativecommons.org/licenses/by/4.0/>.

© The Author(s) 2023